Insights into the improvement effect of Fe doping into the CeO$_2$ catalyst for vapor phase ketonization of carboxylic acids

Feipeng Lu, BinBo Jiang*, Jingdai Wang, Zhengliang Huang, Zuwei Liao, Yongrong Yang

State Key Laboratory of Chemical Engineering, College of Chemical and Biological Engineering, Zhejiang University, Hangzhou 310027, PR China

ARTICLE INFO

ABSTRACT

The conversion of carboxylic acid through ketonization process reduces O-atoms and increases C—C bonds, which can provide attractive routes for upgrading biomass feedstocks into biofuels. The key factors influencing the surface ketonization activity over CeO$_2$-based oxides catalysts remain matters of active discourse. Here, a series of Ce$_{1-x}$Fe$_x$O$_{2-\delta}$ catalysts were investigated for vapor-phase ketonization of acetic and propionic acid. The catalysts were characterized in detail using various physico-chemical techniques both before and after reaction to gain understanding of the ketonization process. The turnover frequency (TOF) based on the basic sites changed with the Fe content. The Ce$_{0.8}$Fe$_{0.2}$O$_{2-\delta}$ sample showed the prominent ketonization activity with the highest TOF value. On one hand, for samples with a lower Fe addition (x < 0.3), the formed CeO$_2$-like solid solution with numerous Ce-O-Fe species showed a dramatic increase in surface oxygen vacancies. These oxygen vacancies were beneficial to catalytic performance. Moreover, the superior redox properties with weaken M—O bonds of Ce-O-Fe species thereby promote the ketonization activity. On the other hand, the higher Fe addition (x > 0.3) caused the damage of the Ce-O-Fe structure, thus reducing ketonization activity. Notably, the investigation of the reaction temperature regime of Ce$_{0.8}$Fe$_{0.2}$O$_{2-\delta}$ sample directly proved the existence of surface redox cycle during the ketonization process.

© 2017 Published by Elsevier B.V.

1. Introduction

Due to the unsustainable consumption of fossil fuel, bio-fuels used for transportation has received considerable attention for the production of energy [1]. As a well-known renewable feedstock, lignocellulosic biomass has already been extensively used in the production of liquid fuels. Fast pyrolysis, a low cost and efficient pathway, is usually applied in converting the lignocellulosic biomass to bio-oil which can be further upgraded into liquid fuels [2,3]. However, pyrolysis derived bio-oil has a high oxygen content with low energy density and compounds with short carbon chain lengths. Due to the poor quality of bio-oil, it is crucial to remove substantial oxygen content and form new C—C bonds, thus improving the total energy density of the bio-fuels [4–6]. Meanwhile, carboxylic acids that accounts for large proportion in the bio-oil (as high as 12 wt%) cause serious corrosion issues during the storage, transport and bio-oil upgrade. Ketonization, a reaction that couples two carboxylic acid molecules into ketone, carbon dioxide and water (Eq. (1)), will be attractive and suitable for the bio-oil upgrading process as it can decrease the oxygen content of bio-

oil without adding hydrogen, increase the carbon chain lengths of small molecules, and simultaneously remove the corrosive acids. This reaction is also considered to be environmentally benign since non-polluting by-products are formed.

$$2RCOOH \rightarrow R_2CO + CO_2 + H_2O \qquad (1)$$

Ketonization reactions of carboxylic acids have been found to be catalyzed by massive metal oxides at a high temperature range of about 300–500 °C [7–11]. CeO$_2$-based oxides were regarded as the preferable catalysts for surface ketonization reaction due to their prominent activity and stability [12–15]. Hasen et al. [16] investigated the catalytic ketonization behaviors over CeO$_2$ by FTIR in comparison to other oxides such as TiO$_2$ and Al$_2$O$_3$. It was concluded that the catalytic centers were identified as reducible Lewis acid-base pair sites and the superior activity of CeO$_2$ was probably caused by its easier reduction properties. Furthermore, different CeO$_2$-based catalysts such as CeO$_2$-Al$_2$O$_3$ [8,9,17], CeO$_2$-MgO [7], CeO$_2$-Mn$_2$O$_3$ [7,18], CeO$_2$-Fe$_2$O$_3$ [7,17], CeO$_2$-TiO$_2$ [19] and CeO$_2$-ZrO$_2$ [5,7,10,18,20–22] have been developed for ketonization of carboxylic acid, and the ketonization activity was largely improved by the modified CeO$_2$ oxides. Nagashima et al. [7] have reported that modified CeO$_2$ samples (Ce-Mg, Ce-Fe, Ce-Mn, etc.) showed higher ketonization activity than pure CeO$_2$. The observed increase activity was thought to be caused by the formation of solid solu-

---

tions. The Zr-doped CeO_2 has recently been used as an efficient ketonization catalyst. The activity enhancement is likely due to the solid solution with abundant Lewis acid-base M-O (M = Ce, Zr) sites and oxygen vacancies. The introduction of ZrO_2 could also result in a lower reduction temperature of the bulk ceria and thus enhanced redox properties [22,23]. Actually, it is generally believed that the surface ketonization mechanism involves consecutive reduction-oxidation cycles of the amphoteric oxides [7,24]. Hence, the catalyst redox properties are assumed to be critical to the improvement of ketonization activity. Despite the above reports, the underlying reasons of the promotional effect of doped CeO_2 catalysts especially for the role of solid solution were not well understood so far. Furthermore, the redox cycle during the ketonziation reaction has not been verified experimentally. Whether the redox properties of CeO_2-like amphoteric oxides are key in maintaining the high ketonization activity is still not very clear.

Giving the issues raised above, the current work focused on exploring the structure-activity relationship of mixed oxides and the role of solid solution during the surface ketonization process. To achieve these purposes, we prepared a series of Ce-Fe solid solutions and then the as-prepared catalysts were applied in the vapor-phase ketonization reaction of carboxylic acid. As is well known, Fe-modified ceria systems present a remarkable improvement of their oxygen exchange abilities as compared with the pure CeO_2, which is due to the strong interaction of Fe and Ce species and the formation of solid solution with different physical and chemical properties [25]. Ce-Fe mixed oxides as heterogeneous catalysts for ketonization reaction can be easily separated from the products and used in continuous-flow fixed-bed process, which is suitable for large-scale industrial application [26,27]. Herein, the catalytic performances of the as-prepared samples were correlated with the observed structural evolution of the catalysts. Besides, the spent catalysts were carefully characterized and analyzed. Our results can furnish fresh perspective on the development of high-efficient heterogeneous catalysts for vapor-phase ketonization reaction and provide new grounds for the following fundamental and applied research using such CeO_2-based mixed oxides catalysts.

2. Experimental details

2.1. Catalyst preparation

$Ce_{1-x}Fe_xO_{2-\delta}$ mixed oxide catalysts were prepared by a general co-precipitation method and x just denotes the molar ratio of Fe/(Ce + Fe) (x = 0.1, 0.2, 0.3, 0.5, 0.7). Solution A was prepared by dissolving appropriate amounts of Fe $(NO_3)_3 \cdot 6H_2O$ and Ce $(NO_3)_3 \cdot 6H_2O$ in the desired molar ratio. Solution B was prepared by dissolving ammonia water (25–28 wt.%) in 100 mL deionized water. In a typical procedure, solutions A and B were added at the same time to a beaker containing 100 mL of deionized water while stirring. The pH of the suspensions was maintained around 9 and then the solution was aged at 70 °C for 4 h. The obtained precipitates were filtered off, washed with distilled water three times and subsequently dried at 90 °C overnight. Finally, the dried sample was calcined at 500 °C for 2 h in the air at a heating rate of 5 °C min^{-1}. Pure CeO_2 and Fe_2O_3 were also prepared for comparison by adopting the same method. The raw chemicals used in this study were purchased from Sinopharm Chemical. Reagent Co. Ltd., China and of analytical reagent grade.

2.2. Catalyst characterization

The powder X-ray diffraction (XRD) patterns of samples were recorded on a Philips PW3050/60 vertical goniometer using Ni-filtered Cu Kα1 radiation (λ = 1.5406 Å). Transmission electron

microscopy (TEM) study was performed on Tecnai F20 instrument operating at 120 kV and 200 kV. The BET surface area, pore volume, and pore size distribution measurements were performed using a Quantachrome Autosorb-iQ instrument. Raman spectra were obtained on an ultraviolet high-resolution Raman spectrometer with a He-Cd laser of excitation wavelength 514.5 nm, which consisted of two accumulations of 30 s with a resolution of 2 cm^{-1}.

Temperature-programmed reductions by hydrogen (H_2-TPR) were recorded using a thermal conductivity detector and a reduction gas of 10 vol.% H_2 in Ar, set at a flow rate of 40 mL/min. Approximately 50 mg samples were pre-treated at 450 °C for 60 min in pure He, then the sample cell was purged with H_2/Ar mixture for 30 min and the analysis ran from 50 °C to 900 °C at a heating rate of 10 °C/min. Water produced by the reduction was trapped in an ice bath upstream of the TCD detector. The sample after a TPR run was reoxidized and then a second TPR run was conducted in order to reveal the redox properties of the sample. The first run was performed up to 900 °C, and then the sample was cooled to a desired temperature (100, 300, 500 °C). Thereafter, the reduced sample was exposed to air at 100, 300, 500 °C for 30 min. Then, the sample was cooled down to 50 °C in air for the second TPR experiment.

The number and the strength of the basic sites of the samples were obtained from temperature-programmed desorption (TPD) of CO_2 pre-adsorbed at room temperature on a Quantachrome Instrument. Approximately 100 mg samples were outgassed and dried at 450 °C for 30 min under 40 mL/min He flow, cooled to room temperature, and then treated with a flow of 10% vol.%CO_2/Ar (40 mL/min) for 120 min. The sample cell was then evacuated for 15 min and purged with He (40 mL/min) for 60 min to remove the physisorbed CO_2. The sample was then heated from room temperature to 500 °C at 10 °C/min. The resulting CO_2 peak was quantified by calculating the areas under the curve on the basis of the known amounts of CO_2 using thermal conductivity.

X-ray photoelectron spectroscopy (XPS) measurements were performed in an Escalab 250Xi with a monochromatized Al K source (1486 eV). Narrow spectra were collected with pass energy of 30 eV. The charge correction was made considering that the C1 s signal of contaminating carbon (C—C or C—H bonds) was centered at 284.8 eV. All samples were dried before the XPS test. A Fourier transform IR spectrometer (NICOLET 5700, USA) was used to acquire the IR spectra of the samples. KBr was used to make the samples for FTIR analysis. TG/DTA (Thermogravimetric/Differential Thermal Analysis) experiments were performed using a Mettler TGA (Thermogravimetric Analysis) system from room temperature to 600 °C at 10 °C/min under N_2 flow (30 mL/min).

Inductively coupled plasma atomic emission spectrometer (ICP-AES) (Thermo iCAP6300) was used to measure the bulk Fe/(Ce + Fe) ratios in the fresh samples. For the analysis, about 10 mg of the catalyst was dissolved in an aqua regia solution. Afterward, the solution was diluted to 500 mL using distilled water and 10 mL of this solution was used for analysis.

2.3. Catalyst testing

The gas-phase ketonization of carboxylic acids was carried in a down-flow quartz fixed-bed reactor (9 mm i.d.) under atmospheric pressure. A HPLC pump was used to introduce the liquid feed solution into the reactor. In a typical run, 0.3 g of catalyst (40–60 mesh) was loaded into the reactor between two plugs of quartz wool and fused SiO_2 granules and the reaction was carried out with liquid acetic acid or propionic acid flow rate of 1.8 mL/h with an N_2 flow rate of 40 mL/min. Each sample was pre-treated in N_2 flow at the lowest reaction temperature for 2 h prior to the reaction. The feed and gas-phase reaction mixtures were analyzed with online GC analysis equipped with two columns in

parallel and two detectors to obtain reactant conversion and product selectivity. The outlet line was heated to 180 °C also with the injection valve of the gas chromatograph to avoid product condensation. Organic compounds were analyzed using a chromatograph equipped with a flame ionization detector and a FFAP capillary column (30 m × 0.32 mm × 0.5 μm), while gas products were analyzed using a TCD detector with a TDX-01 column. The product composition during the continuous reaction was determined by on-line GC analysis using an external standard method. Besides, when SiO_2 granules were solely used, a background conversion of 2–3% was detected at the typical reaction condition. The carbon balance was maintained in the range of $100 \pm 5\%$. The ketone selectivity was defined as the percentage of carboxylic acid converted into a particular product taking into account the reaction stoichiometry. Thus, 100% ketone selectivity would mean 1 mol of carboxylic acid converted to form 0.5 mol of the ketone. Turnover frequency (TOF) is defined as a space-time conversion of propionic acid based on the basic site measured by CO_2-TPD, and is calculated as follows:

$$TOF(h^{-1}) = \frac{space - time\ conversion\ of\ propionic\ acid}{number\ of\ surface\ basicities\,(mmol^{-1})\,(catalyst\ weight(g))}$$

3. Results

3.1. Catalyst performance

The vapor-phase ketonization of acetic acid to acetone over Ce-Fe mixed oxides was carried out at the temperature of 330 °C and 350 °C respectively (Scheme S1). The obtained results are shown in Table 1. It can be found that the ketonization activity was remarkably enhanced by the introduction of iron compared with pure oxides and the catalytic performance was dependent on the content of doped Fe. The acid conversion and ketone yield both reached the highest for the $Ce_{0.8}Fe_{0.2}O_{2-\delta}$ sample and then decreased with the further increasing amount of doped Fe. Notably, the $Ce_{0.3}Fe_{0.7}O_{2-\delta}$ catalyst showed the lowest acid conversion and its ketonization activity was even lower that pure CeO_2 and Fe_2O_3. In addition, some other by-products (acetic anhydride and C1–C2 hydrocarbons) were detected with very low selectivity of <2%.

Likewise, the catalytic ketonization of propionic acid to 3-pentanone over $Ce_{1-x}Fe_xO_{2-\delta}$ catalysts at 350–420 °C was also obtained (Scheme S1) and the results were depicted in Fig. 1A and B. The same evolution of ketonization activity influenced by different amount of Fe doped was observed and the $Ce_{0.8}Fe_{0.2}O_{2-\delta}$ sample also presented the best catalytic performance among all catalysts investigated. Obviously, the carboxylic acid with a longer chain length required higher reaction temperature to achieve the same conversion for acetic acid. The acid conversion of propionic acid gradually increased with the increasing reaction temperature, accompanied by a decrease in the selectivity of 3-pentanone when the temperature was higher than 400 °C. In addition, the ICP results of the liquid products showed the trace content of iron or cerium, which means that there was no loss of active phase for $Ce_{1-x}Fe_xO_{2-\delta}$ catalysts during the vapor-phase ketonization reaction. Hence, the $Ce_{1-x}Fe_xO_{2-\delta}$ catalysts should be a sound choice for industrial application.

3.2. Physical properties of $Ce_{1-x}Fe_xO_{2-\delta}$ catalysts

3.2.1. XRD and N_2 physisorption

Fig. 2A illustrates the XRD profiles of various $Ce_{1-x}Fe_xO_{2-\delta}$ mixed oxides. According to the XRD patterns, pure CeO_2 and Fe_2O_3 displayed the pure cubic fluorite phase and hematite-structured α-Fe_2O_3, respectively. Only CeO_2 phase can be observed in the $Ce_{1-x}Fe_xO_{2-\delta}$ samples when x < 0.7. The CeO_2 (111) peak shifted to higher angles with the increasing amount of doping iron (inset in
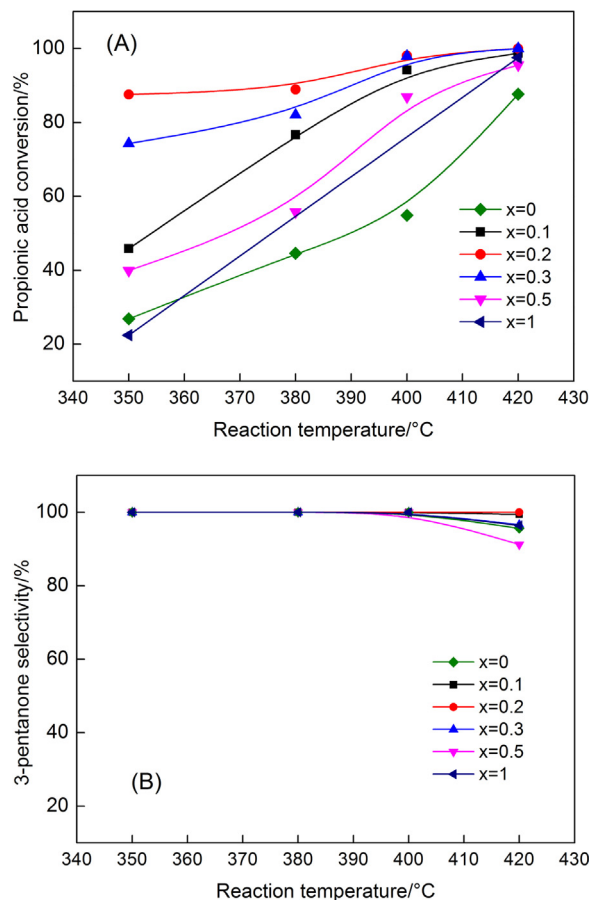

Fig. 1. Propionic acid conversion as a function of temperature for $Ce_{1-x}Fe_xO_{2-\delta}$ catalysts. (Reaction condition: 0.3 g catalyst, 40 mL min^{-1} N_2 flow rate, 0.03 mL min^{-1} liquid flow rate, TOS = 1 h).

Fig. 2A). This phenomenon was attributed to the lattice contraction caused by the introduction of smaller size of the Fe^{3+} cation (0.064 nm) than of the Ce^{4+} cation (0.101 nm) [28,29]. This contraction was evident from the calculated CeO_2 lattice parameters shown in Table 2 and Fig. S1. The lattice parameter decreased linearly from 0.5415 nm to 0.5366 nm when iron content x < 0.2. Although $Ce_{1-x}Fe_xO_{2-\delta}$ catalysts (x > 0.2) also showed a lower lattice parameter compared with the pure ceria, these values did not follow the initial linear law, indicating the limited solubility of Fe_2O_3 in the ceria matrix [28,30]. The diffraction peaks became wider with the doping iron, implying the decrease of the crystallite size (listed in Table 2) which was calculated using the Scherrer equation. Hence, from the above analysis, it can be deduced that an addition of a small amount of Fe_2O_3 into CeO_2 lead the formation of CeO_2-based solid solution. Additionally, the sample with an iron content of 0.7 presented a relatively low intensity of the diffraction peak which demonstrated poor crystallization of the sample. To further confirm the nanostructure of the $Ce_{1-x}Fe_xO_{2-\delta}$ mixed oxides, TEM images and the corresponding SAED patterns of $Ce_{0.8}Fe_{0.2}O_{2-\delta}$ and $Ce_{0.3}Fe_{0.7}O_{2-\delta}$ catalysts are displayed in Fig. 1B–D. The $Ce_{0.8}Fe_{0.2}O_{2-\delta}$ sample was composed of nanosized particles with high crystallinity and the d-spacing value at around 0.312 nm was similar to that of (110) plane of CeO_2. This phenomenon was consistent with cell parameters listed in Table 2, further confirming the formation of CeO_2-based solid solution. The continuous rings in the SAED pattern in Fig. 1C stood for the lattice face of {111}, {200}, {220}, and {311} for CeO_2 from inside and out. In contrast, no circles but several dots were observed for $Ce_{0.3}Fe_{0.7}O_{2-\delta}$ catalyst, giving the direct evidence of its main amor-

Table 1
Ketonization of acetic acid over $Ce_{1-x}Fe_xO_{2-\delta}$ catalysts[a].

Catalyst	Conversion at 330 °C (%)	Selectivity (%) [b]		Conversion at 350 °C (%)	Selectivity (%)	
		Acetone	Others [c]		Acetone	Others
None	–	–	–	2.0	100	0
CeO_2	61.2	100	0	72.9	99.5	0.5
$Ce_{0.9}Fe_{0.1}O_{2-\delta}$	84.5	100	0	97.3	100	0
$Ce_{0.8}Fe_{0.2}O_{2-\delta}$	90.2	99.5	0.5	99.7	99.0	1.0
$Ce_{0.7}Fe_{0.3}O_{2-\delta}$	88.4	99.3	0.7	97.8	98.9	1.1
$Ce_{0.5}Fe_{0.5}O_{2-\delta}$	80.3	99.0	1.0	96.2	98.5	1.5
$Ce_{0.3}Fe_{0.7}O_{2-\delta}$	17.6	99.0	0.5	31.9	99.1	0.8
Fe_2O_3	33.9	100	0	59.7	99.8	0.2

[a] Reaction condition: WHSV (weight hourly space velocity) = 6.7 h^{-1}, Feed rate = 0.03 mL/min, N_2:40 mL/min,TOS = 1 h.
[b] The selectivity was determined by GC analysis using an external standard.
[c] Others contain acetic anhydride, C1 ~ C2 alkanes and alkenes.; CO and CO_2 not included.
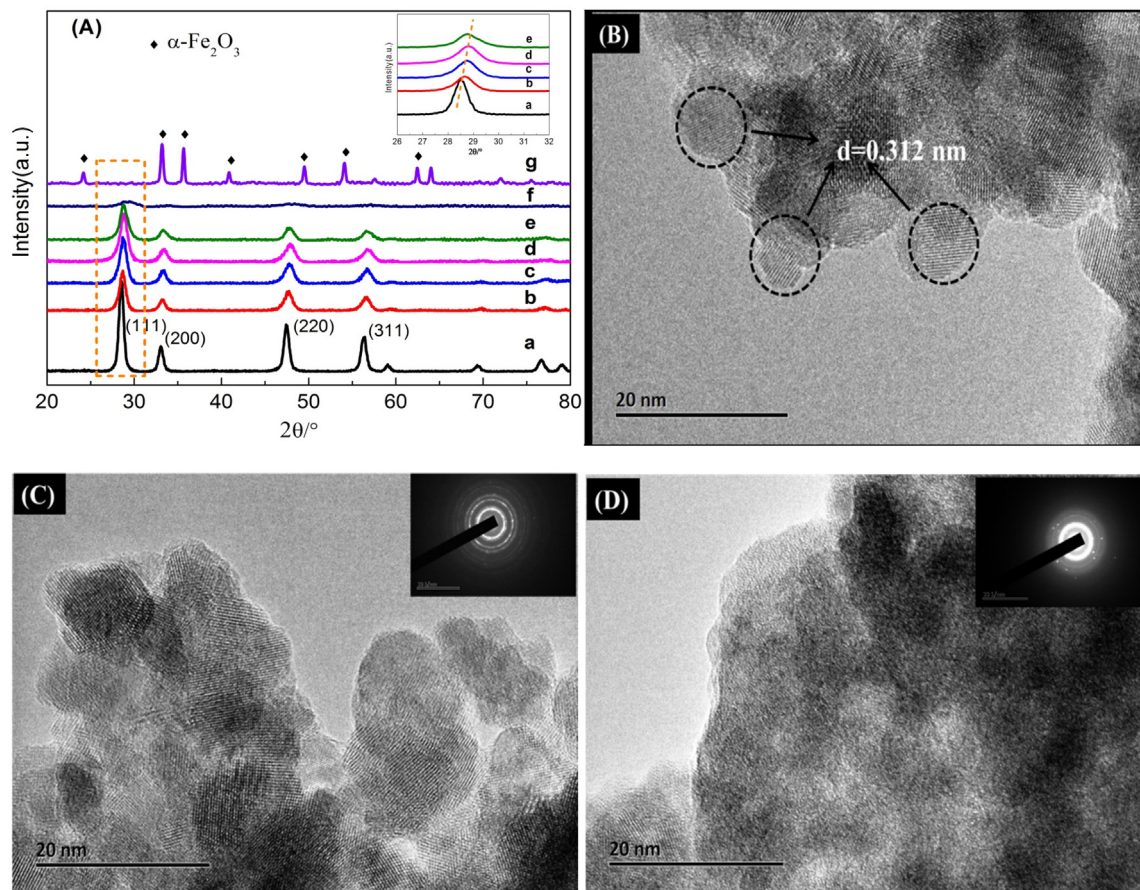
Fig. 2. XRD patterns of (A) as-prepared $Ce_{1-x}Fe_xO_{2-\delta}$ catalysts: (a) x = 0, (b) x = 0.1, (c) x = 0.2, (d) x = 0.3, (e) x = 0.5, (f) x = 0.7, (g) x = 1; TEM images and corresponding SAED patterns (inset) of (B–C) $Ce_{0.8}Fe_{0.2}O_{2-\delta}$ and (D) $Ce_{0.3}Fe_{0.7}O_{2-\delta}$ samples.

Table 2
physical properties, crystalline structure, and crystallite size of $Ce_{1-x}Fe_xO_{2-\delta}$ catalysts.

Catalysts	$2\theta/°$	Lattice parameter(nm)	D(nm)[a]	BET(m^2/g)	Pore diameter(nm)	Pore volume(cm^3/g)
CeO_2	28.516	0.5415	12.6	74	8.2	0.142
$Ce_{0.9}Fe_{0.1}O_{2-\delta}$	28.648	0.5393	9.2	116	24.3	0.381
$Ce_{0.8}Fe_{0.2}O_{2-\delta}$	28.791	0.5366	8.0	93	10.1	0.281
$Ce_{0.7}Fe_{0.3}O_{2-\delta}$	28.869	0.5352	7.7	98	4.7	0.347
$Ce_{0.5}Fe_{0.5}O_{2-\delta}$	28.890	0.5348	7.8	101	5.8	0.262
$Ce_{0.3}Fe_{0.7}O_{2-\delta}$	–	–	–	153	6.8	0.324
Fe_2O_3	–	–	–	34	18.8	0.188

[a] Calculated from the line broadening of the (111) reflection of CeO_2 by the Scherrer equation.

phous structure. The dots can be attributed to the very small size of Fe_2O_3 crystal grains which cannot be detected in the XRD.

The N_2 adsorption-desorption isotherms of $Ce_{1-x}Fe_xO_{2-\delta}$ mixed oxides along with those of CeO_2 and Fe_2O_3 single oxides are shown in Fig.S2. The results of N_2 adsorption-desorption analysis are summarized in Table 2. All the isotherms are type IV with a type H3 hysteresis loop at high relative pressures, which is indicative of the presence of slit-like mesopores associated with aggregates of
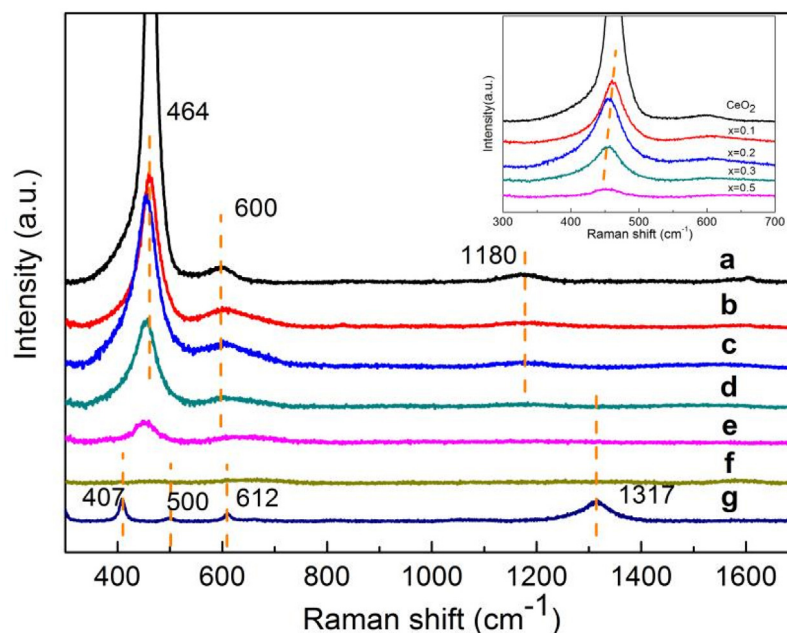
Fig. 3. (A) Raman spectra of various $Ce_{1-x}Fe_xO_{2-\delta}$ catalysts: (a) x = 0, (b) x = 0.1, (c) x = 0.2, (d) x = 0.3, (e) x = 0.5, (f) x = 0.7, (g) x = 1.

plate-like particles. The introduction of Fe into ceria lattice and the as-formed solid-solution obviously increased the surface area of the $Ce_{1-x}Fe_xO_{2-\delta}$ mixed oxides compared to the pure oxides. The $Ce_{0.3}Fe_{0.7}O_{2-\delta}$ sample presented the highest surface area and this can be related to its amorphous structure [31].

The bulk and surface compositions of the $Ce_{1-x}Fe_xO_{2-\delta}$ catalysts were studied by the ICP, XPS and EDS analyses, and the results are summarized in Table S1. The ICP analysis showed that the catalysts had almost the same Fe contents as the initial compositions. The XPS results indicated that Fe components were enriched on the surface for samples with low Fe contents (x ≤ 0.3), while the samples with high Fe contents (x > 0.3) presented lower Fe content on the surface as compared with the bulk ratios. This may be due to the interstitial Fe^{3+} in the CeO_2 lattice at higher Fe content replacing the substitutional Fe^{3+} and these interstitial Fe species mainly located in the bulk of the catalysts [25,30]. From the EDS analysis of the labeled spots in Fig. S3, the Fe/(Ce + Fe) ratios of $Ce_{0.8}Fe_{0.2}O_{2-\delta}$ and $Ce_{0.3}Fe_{0.7}O_{2-\delta}$ were similar to the bulk composition.

3.2.2. Raman

The Raman spectra of $Ce_{1-x}Fe_xO_{2-\delta}$ catalysts are displayed in Fig. 3. Pure CeO_2 exhibited a broad band with a high intensity at ca. $464\,cm^{-1}$, corresponding to the F_{2g} Raman active mode in metal dioxides with fluorite-like structure [25,32]. Besides, a weak band at $1180\,cm^{-1}$ was also observed which was ascribed to the primary A_{1g} asymmetry of CeO_2 [33]. The Fe_2O_3 sample presented the typical bands at 407, 500, 612 and $1317\,cm^{-1}$ as α-Fe_2O_3 [34]. The addition of Fe led to a gradual attenuation of the F_{2g} band intensity. This result may because of the decrease in the amount of Ce as well as the crystalline size of CeO_2 [30]. It is worth mentioned that the band ascribed to the F_{2g} mode of CeO_2 moved to the lower wavenumber regions as depicted in the inset in Fig. 3, which confirmed that the Fe^{3+} has been incorporated into the ceria networks. Moreover, these red-shifts for $Ce_{1-x}Fe_xO_{2-\delta}$ samples could be related to the longer M-O bonds [35], indicating that the doped Fe ions efficiently weakened the M-O bond in the $Ce_{1-x}Fe_xO_{2-\delta}$ solid solution. $Ce_{0.3}Fe_{0.7}O_{2-\delta}$ sample showed no evident Raman bands and this was likely due to its amorphous structure with fine crystal grains which was verified by the XRD and TEM results.

Table 3
Chemical composition and properties of samples.

Catalysts	Raman I_{600}/I_{464}	$Ce^{3+}/(Ce^{3+} + Ce^{4+})/\%$ [a]	Number of total basic sites/mmol/g
CeO_2	0.058	13.3	0.165
$Ce_{0.9}Fe_{0.1}O_{2-\delta}$	0.249	18.0	0.231
$Ce_{0.8}Fe_{0.2}O_{2-\delta}$	0.271	23.7	0.246
$Ce_{0.7}Fe_{0.3}O_{2-\delta}$	0.201	18.1	0.219
$Ce_{0.5}Fe_{0.5}O_{2-\delta}$	0.022	16.6	0.139
$Ce_{0.3}Fe_{0.7}O_{2-\delta}$	–	15.2	0.134
Fe_2O_3	–	–	0.070

[a] values measured by XPS.

The band at $\sim600\,cm^{-1}$ assigned to the production of oxygen vacancies in the fluorite structure was observed [28,30,36]. The oxygen vacancy concentration of the $Ce_{1-x}Fe_xO_{2-\delta}$ catalysts estimated by the intensity ratio of the band at 600 and $464\,cm^{-1}$ (I_{600}/I_{464}) is shown in Table 3. The I_{600}/I_{464} evidently increased with the content of Fe until the maximum for the $Ce_{0.8}Fe_{0.2}O_{2-\delta}$ sample was reached and then decreased with more Fe introduced into the CeO_2 lattice.

3.3. XPS investigation

The XPS analysis was performed to elucidate the transformation of chemical bonding and oxidation states for the $Ce_{1-x}Fe_xO_{2-\delta}$ catalysts. Fig. 4A and B show the Ce3d and Fe2p XPS spectra, respectively. The surface Ce^{3+} ratio (Table 3) was calculated by $Ce^{3+}/(Ce^{3+} + Ce^{4+})$ according to the Ce3d spectra [37]. For $Ce_{1-x}Fe_xO_{2-\delta}$ samples, the Ce^{3+} ratio was higher than that of pure CeO_2. The Ce^{3+} ratio increased with increasing x when x < 0.3. This surface partial reduction of Ce^{4+} for Fe-doped samples can be attributed to the formation of Fe-O—Ce species. The peak positions at 710.8 eV and 723.7 eV were attributed to Fe 2p3/2 and Fe 2p1/2 photoemission lines for each Fe-containing sample respectively, indicating that the iron species in these samples were in Fe^{3+} oxidation state [38]. However, the corresponding binding energies showed no variation, manifesting that the imparity of ketonization
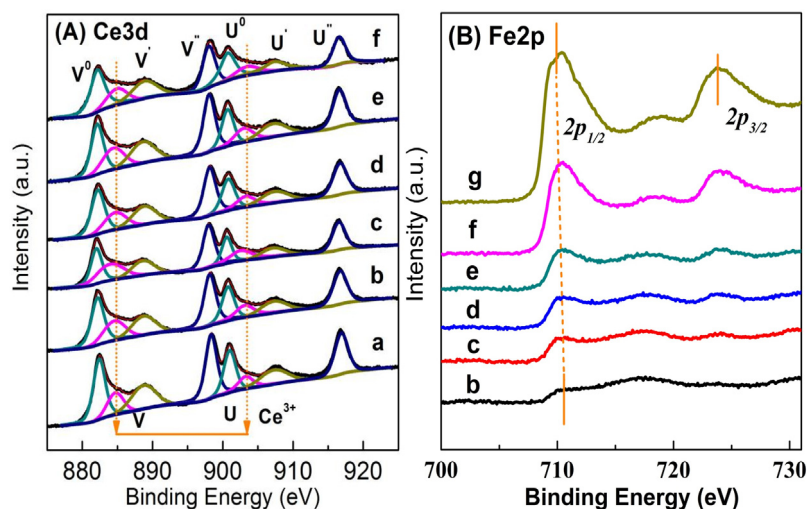
Fig. 4. XPS spectra of $Ce_{1-x}Fe_xO_{2-\delta}$ catalysts: (a) x = 0, (b) x = 0.1, (c) x = 0.2, (d) x = 0.3, (e) x = 0.5, (f) x = 0.7, (g) x = 1.
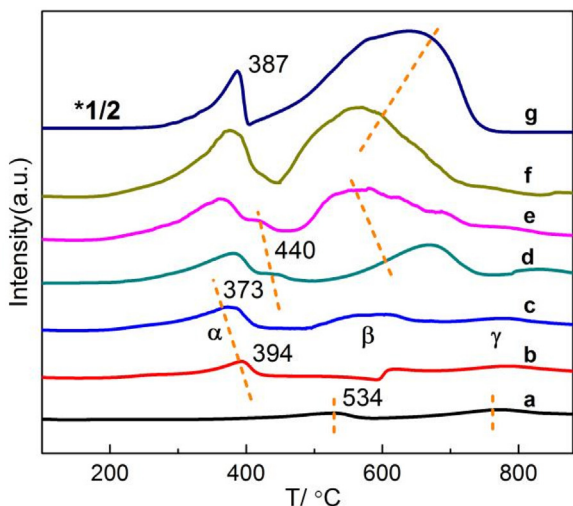
Fig. 5. H_2-TPR profiles $Ce_{1-x}Fe_xO_{2-\delta}$ catalysts: (a) x = 0, (b) x = 0.1, (c) x = 0.2, (d) x = 0.3, (e) x = 0.5, (f) x = 0.7, (g) x = 1.

activities over these catalysts was not caused by the redox ability change of iron species.

3.4. Redox behavior

Fig. 5 shows the H_2-TPR profiles of the $Ce_{1-x}Fe_xO_{2-\delta}$ catalysts. The CeO_2 showed two reduction peaks and the low-temperature peak at 534 °C was owing to the reduction in the surface region of oxides [39,40], as well as the high-temperature peak at 782 °C assigned to the reduction of bulk CeO_2. Single Fe_2O_3 oxide displayed two strong reduction peaks at ca. 387 and 680 °C. The sharp peak at 387 °C was attributed to the reduction of Fe_2O_3 to Fe_3O_4, and the broad peak at 680 °C with high H_2 consumption was corresponding to the reduction of Fe_3O_4 to FeO and Fe^0 [41,42]. The reduction properties of $Ce_{1-x}Fe_xO_{2-\delta}$ catalysts were substantially different from the single metal oxides. The $Ce_{1-x}Fe_xO_{2-\delta}$ samples presented three reduction peaks, labeled α, β and γ. The α peak was related to the reduction of Fe^{3+} in the as-formed solid solution, the β peak at ca. 600 °C could be associated with the reduction of Fe^{2+} and the γ peak at >700 °C should be due to the reduction of bulk Ce^{4+}. It can be seen that the reduction onset temperatures of all the Ce-Fe mixed oxides were much lower than that of either CeO_2 or

Fe_2O_3. This shift in reduction temperatures of Ce-Fe mixed oxides can be related to the formation of solid solution which caused by the synergy between Ce and Fe cations [29]. For $Ce_{1-x}Fe_xO_{2-\delta}$ catalysts (x ≤ 0.2), the as-formed Ce—O—Fe bonds behaved better redox properties than the Ce—O—Ce bonds. The TPR peaks moved to lower temperature in contrast with pure CeO_2, implying the introduction of Fe into the CeO_2 lattice enhanced the reducibility of bulk oxygen and resulted in high efficiency of the $Ce^{4+}\leftrightarrow Ce^{3+}$ redox cycle especially for a CeO_2-rich solid solution. It can be seen that another minor peak at 440 °C emerged between α and β peaks for samples with high Fe content (x ≥ 0.3). Nevertheless, no other structures appeared as suggested by the XRD and Raman results. Therefore, it can be concluded that the peak at around 400 °C reflected the reduction of surface CeO_2, whereas this reduction peak for $Ce_{1-x}Fe_xO_{2-\delta}$ oxides (x ≤ 0.2) was overlapped.

3.5. The surface basicity of $Ce_{1-x}Fe_xO_{2-\delta}$ catalysts

It is believed that the basic property of the catalysts plays an important role in ketonization reaction. Hence, TPD of CO_2 adsorbed on the $Ce_{1-x}Fe_xO_{2-\delta}$ samples was measured to characterize the basicity. As depicted in Fig. S4, a large amount of desorbed CO_2 was only detected during low temperature of ca. 120 °C on pure CeO_2, indicating that CeO_2 had only weak basic sites [43]. Pure Fe_2O_3 presented a broad peak but with a significant lower amount of CO_2 released than that of the pure CeO_2. The incorporation of Fe into the CeO_2 lattice obviously changed the CO_2-TPD profiles of the catalysts. The $Ce_{1-x}Fe_xO_{2-\delta}$ samples had two desorption peaks, at around 100 and 250 °C, implying that the doped Fe produced a number of strong basic sites compared with pure CeO_2. The amount of CO_2 desorbed up to 500 °C was defined as the total number of basic sites and the results were listed in Table 3. The number of basic sites of the $Ce_{1-x}Fe_xO_{2-\delta}$ samples reached a maximum of 0.245 mmol/g when x = 0.2.

3.6. Identification of the reaction temperature regime

3.6.1. The ketonization performance at different reaction temperatures

It can be concluded from the investigation on the catalyst performance that the reaction temperature has a great influence on the ketonization reaction activity (see Table. 1 and Fig. 1). For the reason that the vapor-phase reaction always required a relatively high temperature, almost all the gas-phase ketonization reactions
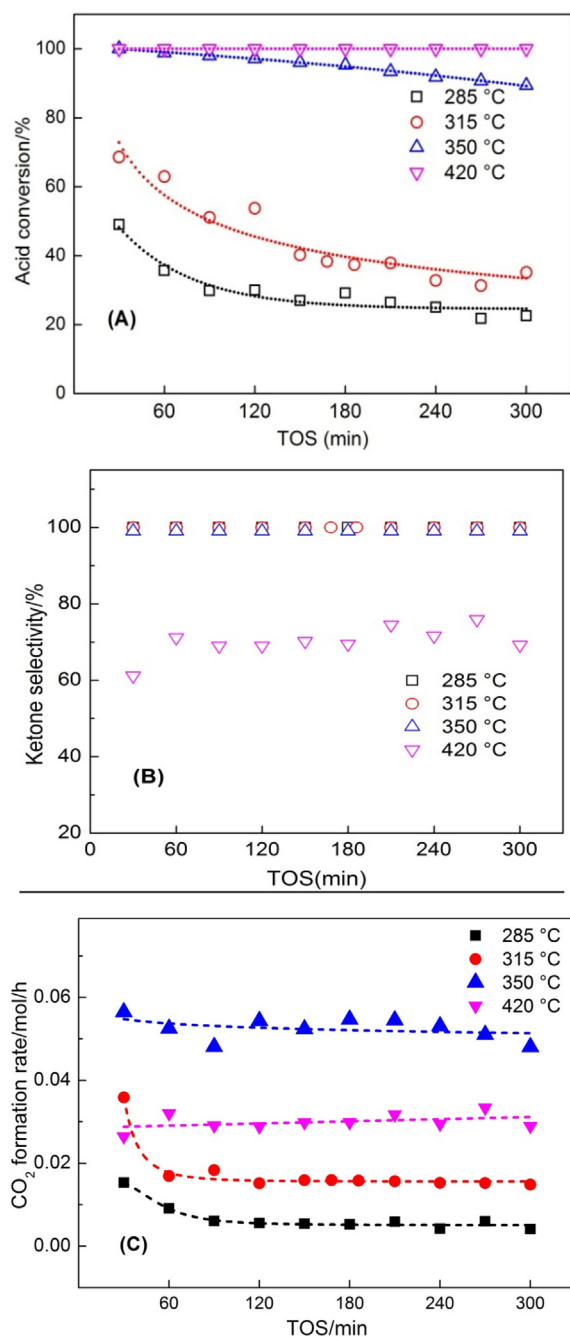
Fig. 6. Acetic acid conversion (A), ketone selectivity (B) and CO_2 formation rate (C) over $Ce_{0.8}Fe_{0.2}O_{2-\delta}$ catalyst reacted at different temperatures. (0.3 g catalyst, 40 mL min^{-1} N_2 flow rate, 0.03 mL min^{-1} liquid flow rate).

took place at above 350 °C [8,9,44,45]. Therefore, the impact of the reaction temperature on the catalytic stability together with the variation of the catalysts properties was rarely reported by other researchers. The vapor-phase ketonization reactions at four reaction temperatures were investigated with the purpose to obtain a comprehensive understanding of the temperature regime for the surface ketonization reaction.

Fig. 6A and B show the performance of $Ce_{0.8}Fe_{0.2}O_{2-\delta}$ catalyst varied with time on stream at different reaction temperatures. The acid conversion showed no decay for reaction at 420 °C but with poor selectivity (70%) for acetone. A small decline of conversion from 100% to 90% can be observed for reaction at 350 °C. However, the catalyst displayed much worse stability for reaction at <350 °C.

The initial conversion was 68% and then dropped to 31% for reaction at 315 °C, while the acid conversion decreased from 48% to 22% for reaction at 285 °C. Fig. 6C shows the CO_2 formation rate of $Ce_{1-x}Fe_xO_{2-\delta}$ catalyst for 300 min on stream at different temperatures and the results are consistent with the acid conversion data.

For comparison, the influence of reaction temperatures on the reaction behavior of pure CeO_2 was also investigated (Fig. S5). Pure CeO_2 exhibited worse activity and deactivated more rapidly compared with the $Ce_{0.8}Fe_{0.2}O_{2-\delta}$ catalyst. The acid conversion over the CeO_2 catalyst dropped from the initial 75% to the final 38% at 350 °C. For a much lower reaction temperature at 285 °C, the acid conversion decreased quickly in the first 60 min and thereafter maintained at around 10%.

3.6.2. Characterization of spent catalysts after reaction at different temperatures

Fig. S6 shows the FTIR spectra of spent catalysts after reaction at four different temperatures. The location of $\nu_s COO^-$ and ν_{as} COO^- together with the $\Delta_{asy-sym}$ values determined the carboxylate coordination mode. For the ketonization reaction, carboxylic acids firstly adsorbed dissociatively on the surface of the catalysts and one or two oxygen atoms of the formed carboxylates could bind to the metal cations with three possible coordination structures, namely monodentate, chelating and bridging bidentate [24]. It can be seen that two strong absorption peaks (at 1553 and 1446 cm^{-1}) were assignable to $\nu_s COO^-$ and ν_{as} COO^- vibrations of surface acetate species for the spent catalyst reacted at 285 °C while two weak absorption peaks at 1047 and 1020 cm^{-1} were due to the $\delta C-H/\nu$ C–O/ν C–C vibrations of acetates [16]. The $\Delta_{asy-sym}$ was equal to ca. 123 cm^{-1}, implying that the surface carboxylate corresponded to bridging or chelating coordination [13]. Besides, the FTIR absorption peaks for acetate diminished when the reaction temperature was higher than 350 °C.

To further verify the surface variation of the spent catalysts, the XPS analysis was performed and shown in Fig. 7. The C1 s spectra were depicted in Fig. 7A. The C1 s peak at 284.6 eV was attributed to the carbon in C=C while the C1 s peak at 288.6 eV was assigned to a carboxylate carbon [46]. A peak shift from 288.6 eV to 288.3 eV can be observed for reaction temperature decreasing from 350 °C to 285 °C. Notably, the spent catalysts showed totally different reduction degree of the surface Ce cations and the surface Ce^{3+} ratio gradually increased with the decrease of the reaction temperature (shown in Fig. 7B and Table S2). In summary, the reaction temperature had a significant effect on the formation and decomposition of surface carboxylate and this formation of acetate species could be tightly linked to the reduction or oxidization of Ce cations on the catalyst surface.

3.7. Recycle test

It can be seen that the $Ce_{0.8}Fe_{0.2}O_{2-\delta}$ catalyst gradually deactivated (Fig. 6) when reacted at 350 °C. The spent catalysts were characterized by FTIR, XPS and XRD (shown in Fig. S7). The XRD diffraction peaks of the $Ce_{0.8}Fe_{0.2}O_{2-\delta}$ catalyst presented no obvious changes when reacted at >350 °C. So it is speculated that the formation of carboxylate species or coke may cause the deactivation of the catalysts. Besides, the oxidation of the surface cerium cation (Fig. 9) may also lead the decrease of the ketonization activity.

The reusability test of the $Ce_{0.8}Fe_{0.2}O_{2-\delta}$ catalyst was shown in Fig. S8. During the 1 st run, the acid conversion decreased from 100% to 89.8% within 240 min time on stream. The spent catalyst was first regenerated in N_2 flow. The catalyst was then applied for ketonization of acetic acid but the activity was not restored. Subsequently, the reaction activity was not recovered when the used catalyst was regenerated by oxidation with air. The above results indicated that
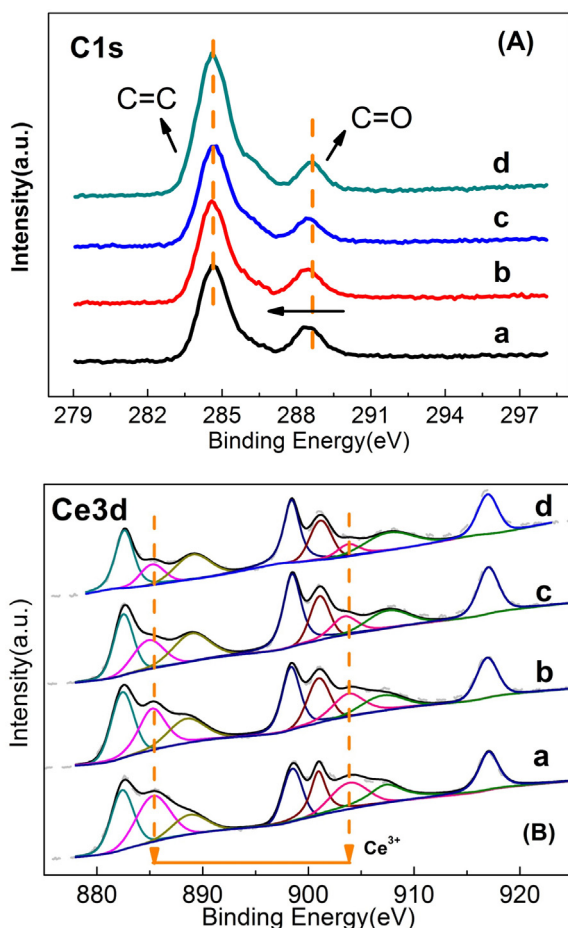
Fig. 7. C1 s (A) and Ce3d (B) spectra of spent catalysts reacted at different temperatures: (a) 285 °C, (b) 315 °C, (c) 350 °C, (d) 420 °C.

the deactivation of the $Ce_{0.8}Fe_{0.2}O_{2-\delta}$ catalyst was not attributed to the formation of carboxylate species or coke.

During the 2nd run, the spent $Ce_{0.8}Fe_{0.2}O_{2-\delta}$ catalyst was reactivated in situ at 450 °C under 10 vol.% H_2 flow (30 mL/min) for 1 h. The ketonization activity could be efficiently restored, which gives the evidence that the catalyst deactivation should be caused by the oxidation of the surface cerium and the spent catalyst can be regenerated by the reduce gas such as H_2.

4. Discussion

Firstly, the performance of the $Ce_{0.8}Fe_{0.2}O_{2-\delta}$ catalyst was compared with the other active catalysts in the recent literatures, and the results are listed in Table 4. The TOF values based on the number of basic sites were also calculated. The $Ce_{0.8}Fe_{0.2}O_{2-\delta}$ catalyst is one of the most promising catalysts for ketonization reaction when taking the activity and ketone selectivity into consideration. Notably, $Ce_{0.8}Fe_{0.2}O_{2-\delta}$ catalyst showed the highest TOF value of $286\,h^{-1}$ among all these catalysts.

From the above characteristic results, it can be seen that the structure of $Ce_{1-x}Fe_xO_{2-\delta}$ catalysts was highly dependent on the Fe content and the structure variation was likely caused by the different interactions between Ce and Fe species. Herein, the relationship between the catalytic properties (oxygen vacancies, redox properties, and so on) and surface ketonization behaviors for all the $Ce_{1-x}Fe_xO_{2-\delta}$ catalysts are discussed in details below.

It is believed that the increasing amount of oxygen vacancies will improve ketonization activity [8,47–51] and this kind of oxygen vacancies or coordinatively unsaturated surface metal cations will facilitate the absorption and activation of acid molecules,

$$CH_3COO- + V_0 \rightarrow CH_3COO-_{(ads),} \tag{2}$$
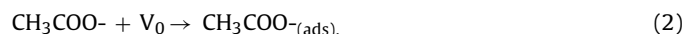
where V_0 denotes the oxygen vacancy. Another trapped acid molecule nearby on the surface would further react with active acid to produce ketone,

$$CH_3COO- + CH_3COO-_{(ads)} \rightarrow (CH_3)_2C=O + COO-, \tag{3}$$
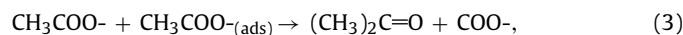
Meanwhile, the ketene-like intermediate will be generated during the acetone formation by the thermally activated loss of α-H of $CH_3COO-_{(ads)}$,

$$(4)\ CH_3COO-_{(ads)} + M-OH \rightarrow CH_2 = COO_{(ads)} +M- +H_2O,$$
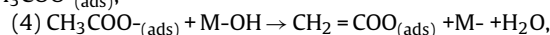
Hence, the TOF value per basic site of Ce-Fe catalysts was correlated with the relative oxygen vacancies concentration (Fig. 8A). It is obvious that the ketonization activity was highly dependent on the surface oxygen vacancy concentration, giving the direct experimental evidence that the creation of oxygen vacancies was beneficial for activating the acid molecules and further ketonization reaction. In fact, these newly generated oxygen vacancies were closely linked to the formation of Ce-O-Fe bonds and created based on the vacancy compensation mechanism [25,30]. The introduction of the Fe atom ($Fe^{3+} \leftrightarrow Fe^{2+}$) as a low-valence dopant compared with Ce atom ($Ce^{4+} \leftrightarrow Ce^{3+}$) into the CeO_2 lattice will make it easier to produce oxygen vacancies, which is due to the reduction of Ce^{4+} by acquiring electrons from Fe cations. Furthermore, it is worth noting that according to the crude electron-pair Lewis theory of the chemical bond, removing an oxygen atom from the surface leaves behind two unpaired electrons which mean that an oxygen vacancy is a

Table 4
Catalytic activity for acid ketonization on different catalysts.

Entry	Catalyst	Conv./%	Select./%	Yield/%	TOF [a]/h^{-1}	Ref.
1	CeO_2	27	100	27	130	This work [b]
2	$Ce_{0.8}Fe_{0.2}O_{2-\delta}$	88	100	88	286	This work [b]
3	MnO_x/CeO_2	80			130	[53] [c]
4	CM-MCM−41[d]	73			88	[53] [c]
5	$CeZrO_x$	50	90	45	6	[22] [e]
6	Ce(9)/ZrO_2			78	178	[54] [f]
7	$Ce_{0.5}Fe_{0.2}Al_{0.3}O_x$		98	91	232	[54] [f]
8	Zn-Cr (10:1)	70	100	70	–	[45] [g]

[a] TOF (h^{-1}) = (mol acid/mol basic sites/h).
[b] Reaction condition: 350 °C, WHSV = 5.9 h^{-1}, propionic acid as feed.
[c] Reaction condition: 410 °C, WHSV = 4.0 h^{-1}, propionic acid as feed.
[d] CM-MCM-41 stands for MCM-41 supported Ce-Mn oxides.
[e] Reaction condition: 270 °C, WHSV = 0.6 h^{-1}, 20 wt.% acetic acid in water.
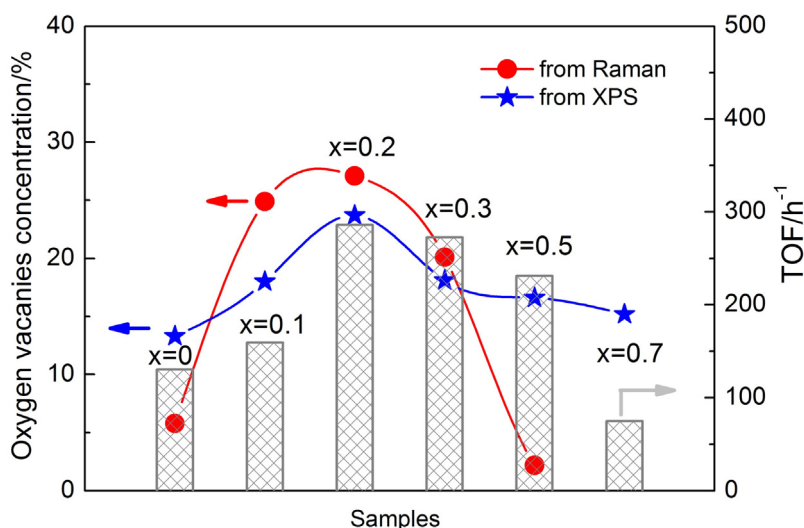[f] Reaction condition: 400 °C, WHSV = 2.0 h^{-1}, acetic acid as feed.
[g] Reaction condition: 350 °C, W/F = 4 h g mol^{-1}, propionic acid as feed.

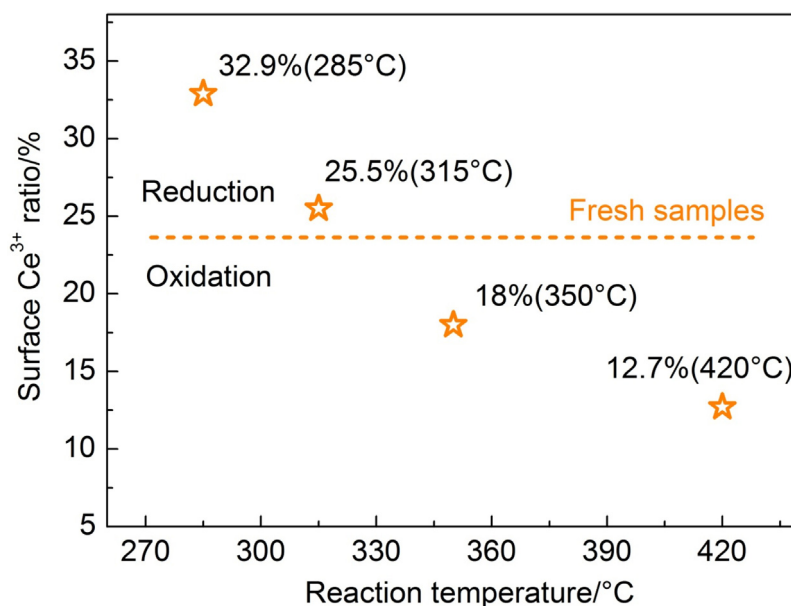**Fig. 8.** Change of TOF values with relative oxygen vacancies concentration.

Fig. 9. Redox cycle of $Ce_{0.8}Fe_{0.2}O_{2-\delta}$ catalyst under different reaction temperatures.

strong Lewis base [52]. That is to say, the doped Fe cations produce not only the oxygen vacancies but also the Lewis basic sites. It can be seen that CO_2 desorbed peak at higher temperature range emerges for Fe-doped CeO_2 samples (Fig. S3), which should be ascribed to the stronger basic sites caused by the formation of Ce-O-Fe species along with oxygen vacancies. These stronger basic sites could also be beneficial for the adsorption process of acid molecule on the catalyst surface [53].

However, the excess amount of doped Fe ($x \geq 0.3$) will change the CeO_2-like solution structures which were testified by XRD, Raman and H_2-TPR. The oxygen vacancies decreased when the content of doped Fe was more than 0.2. A plausible explanation is that the interstitial Fe^{3+} in the CeO_2 lattice at higher Fe content appears instead of the substitutional Fe^{3+}, which is called dopant interstitial compensation mechanism [25,30]. In this case, three Ce^{4+} cations are replaced by three Fe^{3+} cations while one additional Fe^{3+} cation is located in the interstitial sites of the fluorite structure and then neutrality is achieved. In other words, the interstitial Fe^{3+} seemed adverse to the adsorption of carboxylic acid. As a consequence,

the TOF values declined with the increasing amount of Fe content ($x \geq 0.3$).

The above investigation on the ketonization behaviors over Ce-Fe catalysts uncovered that the reaction temperature had a significant effect on the chemical valence of surface Ce species. The surface Ce^{3+} ratios of spent catalysts which reacted at different reaction temperatures were presented in Fig. 9. For the lower reaction temperature (<315 °C), the spent catalysts possessed the higher surface Ce^{3+} ratio than the fresh sample (23.7%), while the higher reaction temperatures caused the oxidation of surface Ce^{3+}. Previous studies have shown that both the "ketene" and "carboxylate" mechanisms of ketonization reaction involve the surface reduction/oxidation process [7,47]. It should be noted that the investigation of reaction temperature regime directly proved the appearance of redox cycle for ketonization over reducible oxides. Based on the mechanism involving β-ketoacid as an intermediate, the as-proposed mechanism is shown in Scheme 1. The dissociative adsorption of the proton from the carboxylic groups of two acids with the formation of surface carboxylates is the first step. Due to
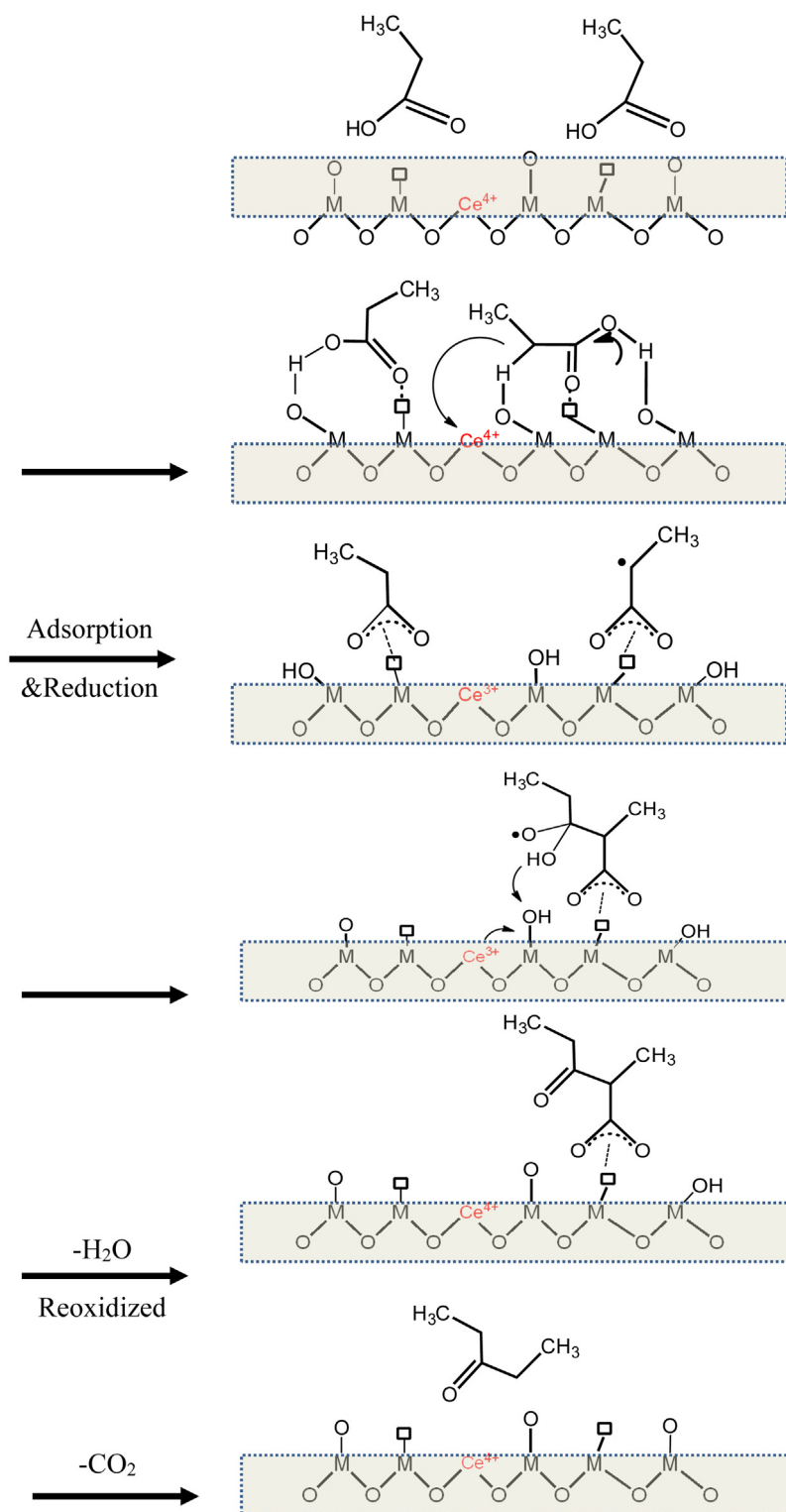
Scheme 1. Proposed surface ketonization mechanism (β-ketoacid as intermediate) for vapor-phase ketonization of propionic acid over the $Ce_{0.8}Fe_{0.2}O_{2-\delta}$ catalyst. (□ stands for oxygen vacancies).

the crucial role of oxygen vacancies in ketonization reaction, the carboxylates prefer to adsorb onto the coordinatively unsaturated sites, namely oxygen vacancies. The α-H atom is then abstracted from one carboxylate and a corresponding anionic radical is formed. Simultaneously, the surface Ce^{4+} cations are partly reduced by picking up the redundant electrons from the abstracted α-H atoms. The anionic radical subsequently attacks another carboxylate to form

the β-ketoacid intermediate, while the Ce^{3+} cations are reoxidized by the hydroxyl radical desorbed from the intermediate. The β-ketoacid intermediates finally decarboxylate to form the ketone product. From the investigation of reaction temperature regime, it can be deduced that the surface reduction dominated during the ketonization process when the reaction took place in a low temperature range. But the as-formed surface carboxylate species were
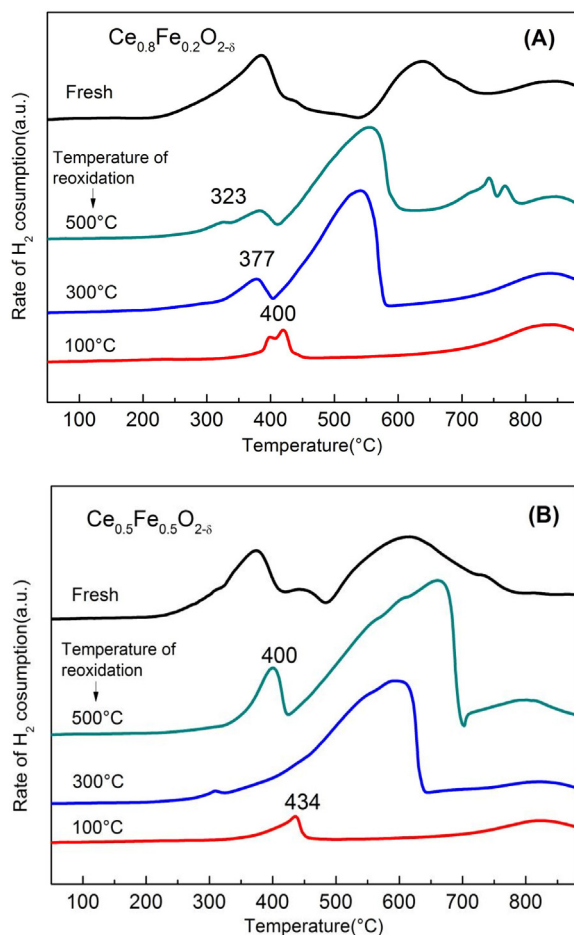
Fig. 10. TPR profiles of the $Ce_{0.8}Fe_{0.2}O_{2-\delta}$ (A) and $Ce_{0.5}Fe_{0.5}O_{2-\delta}$ (B) sample and the reduced sample reoxidized at different temperatures.

decomposed to products and the catalyst surface was then oxidized by the desorbed hydroxyl from the acid as the reaction was carried out in a high temperature range. In this case, the surface oxidation dominated.

Summarizing the above results, we conclude that the redox properties should be emphatically considered to explain the activity differences among all $Ce_{1-x}Fe_xO_{2-\delta}$ catalysts. Fig. 10 shows the repeated TPR cycles of $Ce_{0.8}Fe_{0.2}O_{2-\delta}$ and $Ce_{0.5}Fe_{0.5}O_{2-\delta}$ samples at different reoxidation temperatures. The reduction peaks were very weak after reoxidation at 100 °C for both two samples, whereas $Ce_{0.8}Fe_{0.2}O_{2-\delta}$ sample showed a lower reduction peak at ca. 400 °C. The TPR peak areas of $Ce_{0.8}Fe_{0.2}O_{2-\delta}$ sample reoxidized at 300 and 500 °C were nearly the same. However, for the $Ce_{0.5}Fe_{0.5}O_{2-\delta}$ sample, the reoxidized sample at 300 °C lacked a distinct reduction peak at ca. 400 °C and its reduction peak area was much less than the one reoxidized at 500 °C. In comparison, the three TPR curves for pure CeO_2 were almost the same as the fresh sample (not shown here), indicating that its poor redox property was not affected by the treatment of reduction-oxidation. Besides, the Ce3d XPS of CeO_2 reacted at different temperatures are shown in Fig. S9. It can be seen that the XPS profiles of CeO_2 remained basically identical before and after reaction, suggesting that the strong M-O bonds stabilized the chemical state of surface Ce anion, which impeded the redox cycle during the ketonization process. Therefore, the reason that $Ce_{0.8}Fe_{0.2}O_{2-\delta}$ sample can maintain the high ketonization activity should be tightly associated with its outstanding redox ability. For samples with the excess incorporation of Fe, such as $Ce_{0.5}Fe_{0.5}O_{2-\delta}$, the inferior redox ability led to the worse ketonization activity.

Furthermore, the improved redox ability is also connected with the red-shift of F_{2g} Raman band (Fig. 3) involving the weakened M-O bonds which allows the catalysts to react more easily with the carboxylic acid leading to the formation of carboxylic intermediates [17]. In order to expound how Fe-O-Ce species affected the formation of surface intermediates, the TGA curves of the spent catalysts of both CeO_2 and $Ce_{0.8}Fe_{0.2}O_{2-\delta}$ were acquired (Fig. S10). Decomposition of the 285 and 350 °C catalysts showed that $Ce_{0.8}Fe_{0.2}O_{2-\delta}$ lost much more weight compared with pure CeO_2. Therefore, the more active catalyst with enhanced redox ability displayed the easier formation of metal carboxylate for the vapor-phase ketonization reaction.

It is worth mentioning that the $Ce_{0.3}Fe_{0.7}O_{2-\delta}$ displayed the worst ketonization rate in contrast with other samples. It is conceivable that this phenomenon was caused by the destruction of the as-formed solid solution and Ce—O—Fe linkage bonds and its amorphous structure was confirmed by the XRD, TEM and Raman data. This result further manifested the crucial role of Ce-O-Fe species for the ketonization reaction.

5. Conclusion

The ketonization of acetic and propionic acid has been carried out on the $Ce_{1-x}Fe_xO_{2-\delta}$ (x = 0.1 ∼ 0.7) mixed oxide catalysts. The calculated TOF values were highly dependent on the doping amount of Fe. First, the CeO_2-like solid solution was formed to provide Ce-O-Fe species as active sites for converting carboxylic acid molecules when Fe content is low (x ≤ 0.2). $Ce_{0.8}Fe_{0.2}O_{2-\delta}$ sample which possessed the highest oxygen vacancies concentration and improved reducibility presents the prominent ketonization activity with the highest TOF value. Second, the reaction temperature regime further confirmed that surface redox cycle do exist during the ketonization process. It is beneficial for Ce-O-Fe species which showed superior redox properties with a weaken M-O bonds proceed through the formation and subsequent decomposition of surface carboxylate. So the spent $Ce_{0.8}Fe_{0.2}O_{2-\delta}$ catalyst owned much more surface carboxylate and thus displayed much higher ketonization activity and improved stability compared with pure CeO_2. Third, the decline of TOF values was observed for samples with higher Fe addition (x ≥ 0.3). This was caused by the damage of the solid solution structure as well as Ce—O—Fe linkage bonds.

In summary, the above results indicate that solid solution plays an important role in the formation of Ce-O-Fe species for CeO_2-rich catalysts during the ketonization process. The performance of Fe-CeO_2 catalysts depends on their superior redox properties accompanied by the improved oxygen vacancies content. It is reasonable to conclude that Fe doped CeO_2 materials are suitable for practical application in the ketonization reaction.

Appendix A. Supplementary data

Supplementary data associated with this article can be found, in the online version, at http://dx.doi.org/10.1016/j.mcat.2017.05. 022.

References

[1] D.M. Alonso, J.Q. Bond, J.A. Dumesic, Green. Chem. 12 (2010) 1493–1513.
[2] G.W. Huber, S. Iborra, A. Corma, Chem. Rev. 106 (2006) 4044–4098.
[3] D. Mohan, C.U. Pittman, P.H. Steele, Energ. Fuel 20 (2006) 848–889.

[4] G.W. Huber, A. Corma, Angew. Chem. Int. Edit. 46 (2007) 7184–7201.
[5] E.L. Kunkes, D.A. Simonetti, R.M. West, J.C. Serrano-Ruiz, C.A. Gärtner, J.A. Dumesic, Science 322 (2008) 417–421.
[6] D.A. Bulushev, J.R. Ross, Catal. Today 171 (2011) 1–13.
[7] O. Nagashima, S. Sato, R. Takahashi, T. Sodesawa, J. Mol. Catal. A: Chem. 227 (2005) 231–239.
[8] K.M. Dooley, A.K. Bhat, C.P. Plaisance, A.D. Roy, Appl Catal. A 320 (2007) 122–133.
[9] L. Deng, Y. Fu, Q. Guo, Energ. Fuel 23 (2008) 564–568.
[10] C.A. Gärtner, J.C. Serrano Ruiz, D.J. Braden, J.A. Dumesic, ChemSusChem 2 (2009) 1121–1124.
[11] Y. Yamada, M. Segawa, F. Sato, T. Kojima, S. Sato, J. Mol. Catal. A: Chem. 346 (2011) 79–86.
[12] L. Vivier, D. Duprez, ChemSusChem 3 (2010) 654–678.
[13] R.W. Snell, B.H. Shanks, ACS Catal. 3 (2013) 783–789.
[14] R.W. Snell, B.H. Shanks, Appl. Catal. A 451 (2013) 86–93.
[15] R.W. Snell, S.H. Hakim, J.A. Dumesic, B.H. Shanks, Appl. Catal. A 464 (2013) 288–295.
[16] M.A. Hasan, M.I. Zaki, L. Pasupulety, Appl. Catal. A 243 (2003) 81–92.
[17] R.W. Snell, B.H. Shanks, ACS Catal. 4 (2014) 512–518.
[18] C. Liu, A.M. Karim, V.M. Lebarbier, D. Mei, Y. Wang, Top. Catal. 56 (2013) 1782–1789.
[19] F. Lu, B. Jiang, J. Wang, Z. Huang, Z. Liao, Y. Yang, J. Zheng, RSC Adv. 7 (2017) 22017–22026.
[20] C.A. Gaertner, J.C. Serrano-Ruiz, D.J. Braden, J.A. Dumesic, J. Catal. 266 (2009) 71–78.
[21] Y.A. Zaytseva, V.N. Panchenko, M.N. Simonov, A.A. Shutilov, G.A. Zenkovets, M. Renz, I.L. Simakova, V.N. Parmon, Top. Catal. 56 (2013) 846–855.
[22] S.H. Hakim, B.H. Shanks, J.A. Dumesic, Appl. Catal. B 142 (2013) 368–376.
[23] E.L. Kunkes, E.I. Gürbüz, J.A. Dumesic, J. Catal. 266 (2009) 236–249.
[24] T.N. Pham, T. Sooknoi, S.P. Crossley, D.E. Resasco, ACS Catal. 3 (2013) 2456–2473.
[25] F.J. Pérez-Alonso, M. López Granados, M. Ojeda, P. Terreros, S. Rojas, T. Herranz, J. Fierro, M. Gracia, J.R. Gancedo, Chem. Mater. 17 (2005) 2329–2339.
[26] M. Shokouhimehr, K. Shin, J.S. Lee, M.J. Hackett, S.W. Jun, M.H. Oh, J. Jang, T. Hyeon, J. Mater. Chem. A. 2 (2014) 7593.
[27] K.M. Choi, Y. Shokouhimehr, B. Sung, Korean Chem. Soc. 34 (2013) 1477–1480.
[28] H. Bao, X. Chen, J. Fang, Z. Jiang, W. Huang, Catal. Lett. 125 (2008) 160–167.
[29] O.H. Laguna, M.A. Centeno, M. Boutonnet, J.A. Odriozola, Appl. Catal. B 106 (2011) 621–629.
[30] H. Wang, Z. Qu, H. Xie, N. Maeda, L. Miao, Z. Wang, J. Catal. 338 (2016) 56–67.
[31] Z. Liu, J. Zhu, J. Li, L. Ma, S.I. Woo, ACS Appl. Mater. Inter. 6 (2014) 14500–14508.
[32] G.W. Graham, W.H. Weber, C.R. Peters, R. Usmen, J. Catal. 130 (1991) 310–313.
[33] W.H. Weber, K.C. Hass, J.R. McBride, Phys. Rev. B 48 (1993) 178.
[34] D. De Faria, S. Venâncio Silva, M.T. De Oliveira, J. Raman Spectrosc. 28 (1997) 873–878.
[35] T. Masui, K. Koyabu, K. Minami, T. Egawa, N. Imanaka, J. Phys. Chem. C 111 (2007) 13892–13897.
[36] J.E. Spanier, R.D. Robinson, F. Zhang, S. Chan, I.P. Herman, Phys. Rev. B 64 (2001) 245407.
[37] P. Burroughs, A. Hamnett, A.F. Orchard, G. Thornton, J. Chem. Soc. Dalton Trans. (1976) 1686–1698.
[38] F. Liu, H. He, Y. Ding, C. Zhang, Appl. Catal. B 93 (2009) 194–204.
[39] E. Aneggi, M. Boaro, C.D. Leitenburg, G. Dolcetti, A. Trovarelli, J. Alloy Compd. 408–412 (2006) 1096–1102.
[40] M. Luo, J. Chen, L. Chen, J. Lu, Z. Feng, C. Li, Chem. Mater. 13 (2001) 197–202.
[41] S. Li, A. Li, S. Krishnamoorthy, E. Iglesia, Catal. Lett. 77 (2001) 197–205.
[42] D. Qiao, G. Lu, X. Liu, Y. Guo, Y. Wang, Y. Guo, J. Mater. Sci. 46 (2011) 3500–3506.
[43] Y. Kamimura, S. Sato, R. Takahashi, T. Sodesawa, T. Akashi, Appl. Catal. A 252 (2003) 399–410.
[44] M. Renz, Eur. J. Org. Chem. 2005 (2005) 979–988.
[45] H. Bayahia, E.F. Kozhevnikova, I.V. Kozhevnikov, Appl. Catal. B 165 (2015) 253–259.
[46] J. Zhang, Y.S. Choi, B.H. Shanks, ChemSusChem 8 (2015) 4256–4265.
[47] S.D. Randery, J.S. Warren, K.M. Dooley, Appl. Catal. A 226 (2002) 265–280.
[48] T.N. Pham, D. Shi, T. Sooknoi, D.E. Resasco, J. Catal. 295 (2012) 169–178.
[49] K.S. Kim, M.A. Barteau, J. Catal. 125 (1990) 353–375.
[50] S. Wang, E. Iglesia, J. Catal. 345 (2017) 183–206.
[51] S. Tosoni, G. Pacchioni, J. Catal. 344 (2016) 465–473.
[52] G.N. Lewis, J. Chem. Phys. 1 (1933) 17–28.
[53] A.D. Murkute, J.E. Jackson, D.J. Miller, J. Catal. 278 (2011) 189–199.
[54] M.A. Jackson, S.C. Cermak, Appl. Catal. A 431 (2012) 157–163.